Beyond the neutron drip line: The unbound oxygen isotopes ^{25}O and ^{26}O

C. Caesar,[1,2] J. Simonis,[1,3] T. Adachi,[4] Y. Aksyutina,[2,3] J. Alcantara,[5] S. Altstadt,[6] H. Alvarez-Pol,[5] N. Ashwood,[7] T. Aumann,[1,2,*] V. Avdeichikov,[8] M. Barr,[7] S. Beceiro,[5] D. Bemmerer,[9] J. Benlliure,[5] C. A. Bertulani,[10] K. Boretzky,[2] M. J. G. Borge,[11] G. Burgunder,[12] M. Caamano,[5] E. Casarejos,[13] W. Catford,[14] J. Cederkäll,[8] S. Chakraborty,[15] M. Chartier,[16] L. Chulkov,[17,3] D. Cortina-Gil,[5] U. Datta Pramanik,[15] P. Diaz Fernandez,[5] I. Dillmann,[2] Z. Elekes,[9] J. Enders,[1] O. Ershova,[6] A. Estrade,[2,18] F. Farinon,[2] L. M. Fraile,[19] M. Freer,[7] M. Freudenberger,[1] H. O. U. Fynbo,[20] D. Galaviz,[21] H. Geissel,[2] R. Gernhäuser,[22] P. Golubev,[8] D. Gonzalez Diaz,[1] J. Hagdahl,[23] T. Heftrich,[6] M. Heil,[2] M. Heine,[1] A. Heinz,[23] A. Henriques,[21] M. Holl,[1] J. D. Holt,[24,25] G. Ickert,[2] A. Ignatov,[1] B. Jakobsson,[8] H. T. Johansson,[23] B. Jonson,[23] N. Kalantar-Nayestanaki,[4] R. Kanungo,[18] A. Kelic-Heil,[2] R. Knöbel,[2] T. Kröll,[1] R. Krücken,[22,†] J. Kurcewicz,[2] M. Labiche,[26] C. Langer,[6] T. Le Bleis,[22] R. Lemmon,[26] O. Lepyoshkina,[22] S. Lindberg,[23] J. Machado,[21] J. Marganiec,[3] V. Maroussov,[27] J. Menéndez,[1,3] M. Mostazo,[5] A. Movsesyan,[1] A. Najafi,[4] T. Nilsson,[23] C. Nociforo,[2] V. Panin,[1] A. Perea,[11] S. Pietri,[2] R. Plag,[6] A. Prochazka,[2] A. Rahaman,[15] G. Rastrepina,[2] R. Reifarth,[6] G. Ribeiro,[11] M. V. Ricciardi,[2] C. Rigollet,[4] K. Riisager,[20] M. Röder,[28,9] D. Rossi,[2] J. Sanchez del Rio,[11] D. Savran,[3,29] H. Scheit,[1] A. Schwenk,[3,1] H. Simon,[2] O. Sorlin,[12] V. Stoica,[4,30] B. Streicher,[4] J. Taylor,[16] O. Tengblad,[11] S. Terashima,[2] R. Thies,[23] Y. Togano,[3] E. Uberseder,[31] J. Van de Walle,[4] P. Velho,[21] V. Volkov,[1] A. Wagner,[9] F. Wamers,[1] H. Weick,[2] M. Weigand,[6] C. Wheldon,[7] G. Wilson,[32] C. Wimmer,[6] J. S. Winfield,[2] P. Woods,[33] D. Yakorev,[9] M. V. Zhukov,[23] A. Zilges,[27] M. Zoric,[2] and K. Zuber[28]

(R3B collaboration)

[1]*Institut für Kernphysik, Technische Universität Darmstadt, 64289 Darmstadt, Germany*

[2]*GSI Helmholtzzentrum für Schwerionenforschung, D-64291 Darmstadt, Germany*

[3]*ExtreMe Matter Institute EMMI, GSI Helmholtzzentrum für Schwerionenforschung GmbH, 64291 Darmstadt, Germany*

[4]*KVI, University of Groningen, Zernikelaan 25, NL-9747 AA Groningen, The Netherlands*

[5]*Departamento de Física de Partículas, Universidade de Santiago de Compostela, 15706 Santiago de Compostela, Spain*

[6]*Goethe-Universität Frankfurt am Main, 60438 Frankfurt am Main, Germany*

[7]*School of Physics and Astronomy, University of Birmingham, Birmingham B15 2TT, United Kingdom*

[8]*Department of Physics, Lund University, S-22100 Lund, Sweden*

[9]*Helmholtz-Zentrum Dresden-Rossendorf, D-01328 Dresden, Germany*

[10]*Department of Physics and Astronomy, Texas A&M University-Commerce, Commerce, Texas 75429, USA*

[11]*Instituto de Estructura de la Materia, CSIC, Serrano 113 bis, E-28006 Madrid, Spain*

[12]*Grand Accélérateur National d'Ions Lourds (GANIL), CEA/DSM-CNRS/IN2P3, B.P. 55027, F-14076 Caen Cedex 5, France*

[13]*University of Vigo, E-36310 Vigo, Spain*

[14]*Department of Physics, University of Surrey, Guildford GU2 5FH, United Kingdom*

[15]*Saha Institute of Nuclear Physics, 1/AF Bidhan Nagar, Kolkata 700064, India*

[16]*Oliver Lodge Laboratory, University of Liverpool, Liverpool L69 7ZE, United Kingdom*

[17]*Kurchatov Institute, Ru-123182 Moscow, Russia*

[18]*Astronomy and Physics Department, Saint Mary's University, Halifax, Nova Scotia, Canada B3H 3C3*

[19]*Facultad de Ciencias Fsicas, Universidad Complutense de Madrid, Avenida Complutense, E-28040 Madrid, Spain*

[20]*Department of Physics and Astronomy, Aarhus University, DK-8000 Århus C, Denmark*

[21]*Centro de Fisica Nuclear, University of Lisbon, P-1649-003 Lisbon, Portugal*

[22]*Physik Department E12, Technische Universität München, 85748 Garching, Germany*

[23]*Fundamental Fysik, Chalmers Tekniska Högskola, S-412 96 Göteborg, Sweden*

[24]*Department of Physics and Astronomy, University of Tennessee, Knoxville, Tennessee 37996, USA*

[25]*Physics Division, Oak Ridge National Laboratory, P.O. Box 2008, Oak Ridge, Tennessee 37831, USA*

[26]*STFC Daresbury Laboratory, Daresbury, Warrington WA4 4AD, United Kingdom*

[27]*Institut für Kernphysik, Universität zu Köln, D-50937 Köln, Germany*

[28]*Institut für Kern- und Teilchenphysik, Technische Universität, 01069 Dresden, Germany*

[29]*Frankfurt Institut for Advanced Studies FIAS, Frankfurt, Germany*

[30]*Department of Sociology/ICS, University of Groningen, 9712 TG Groningen, The Netherlands*

[31]*Department of Physics, University of Notre Dame, Notre Dame, Indiana 46556, USA*

[32]*Department of Physics, University of Surrey, Guildford GU2 5XH, United Kingdom*

[33]*School of Physics and Astronomy, University of Edinburgh, Edinburgh EH9 3JZ, United Kingdom*

(Received 2 September 2012; revised manuscript received 13 August 2013; published 16 September 2013)

The very neutron-rich oxygen isotopes ^{25}O and ^{26}O are investigated experimentally and theoretically. The unbound states are populated in an experiment performed at the R3B-LAND setup at GSI via proton-knockout reactions from ^{26}F and ^{27}F at relativistic energies around 442 and 414 MeV/nucleon, respectively. From the kinematically complete measurement of the decay into ^{24}O plus one or two neutrons, the ^{25}O ground-state energy and width are determined, and upper limits for the ^{26}O ground-state energy and lifetime are extracted. In

addition, the results provide indications for an excited state in ^{26}O at around 4 MeV. The experimental findings are compared to theoretical shell-model calculations based on chiral two- and three-nucleon ($3N$) forces, including for the first time residual $3N$ forces, which are shown to be amplified as valence neutrons are added.

DOI: 10.1103/PhysRevC.88.034313 PACS number(s): 21.10.−k, 25.60.−t, 27.30.+t, 29.30.Hs

I. INTRODUCTION

Understanding the properties of nuclei with extreme neutron-to-proton ratios presents a major challenge for rare-isotope beam experiments and nuclear theory. Nuclei located at and beyond the neutron drip line play a crucial role in this endeavor. Experimentally, the neutron drip line has been established up to oxygen [1–3] with ^{24}O being the last bound isotope, while it extends considerably further in fluorine [4]. Recently, it has been shown that the anomalous behavior in the oxygen isotopes is attributable to the impact of three-nucleon ($3N$) forces, which provide repulsive contributions to the interactions of valence neutrons [5], connecting the frontier of neutron-rich nuclei to the theoretical developments of nuclear forces.

Another striking feature in the oxygen isotopic chain is the doubly magic nature of ^{22}O and ^{24}O [6–11] in strong contrast to the lighter elements, where the drip line is marked by nuclei exhibiting a loosely bound halo structure. The neutron-rich oxygen isotopes also provide interesting insights, when viewed coming from their stable isotones. As protons are removed, the attractive contribution from the proton-neutron tensor force decreases, thus opening up the $N = 16$ neutron shell gap for oxygen [12], while reducing the gap at $N = 20$, which is very prominent in stable nuclei.

How the structure evolves beyond ^{24}O towards $N = 20$ is thus of central interest. Currently, ^{25}O and ^{26}O are at the limit of experimental availability. For the former isotope, the ground-state resonance energy and width have been reported [6]. For the latter, its position has been measured previously [13]. Taking advantage of the large angular acceptance for neutrons in the R3B-LAND experiment [14,15], we investigate the unbound isotopes ^{25}O and ^{26}O in an extended energy range with an essentially constant efficiency up to a decay energy of 4 and 8 MeV, respectively.

It has been speculated that the unbound isotopes ^{26}O and ^{28}O might have a rather long lifetime, which would constitute the first example of neutron radioactivity [16]. Our present result establishes an upper limit for the lifetime of the ^{26}O ground state. We then combine the experimental investigation with theoretical calculations based on chiral two-nucleon (NN) and $3N$ forces, where we focus on the increasing contribution from residual three-neutron forces as neutrons are added.

II. EXPERIMENT

The experiment was carried out at the GSI Helmholtzzentrum in Darmstadt using the R3B-LAND reaction setup. Beams of light neutron-rich nuclei were produced by fragmentation reactions of a 490 MeV/nucleon ^{40}Ar primary beam in a 4 g/cm^2 Be target. Ions with a magnetic rigidity of 9.88(±1%) Tm corresponding to an A/Z ratio of about 3 were selected by the fragment separator FRS [17] and transported to the experimental area. Energy-loss and time-of-flight measurements allowed for the identification of the incoming ions on an event-by-event basis. The beam cocktail contained ^{26,27}F ions (∼1%), which were selected to populate the unbound states in ^{25,26}O via one-proton knockout reactions. The energies (intensities) of the ^{26}F and ^{27}F beams were 442 and 414 MeV/nucleon (1 and 0.3 Hz), respectively. Different secondary targets (922 mg/cm^2 CH_2, 935 mg/cm^2 C, and 2145 mg/cm^2 Pb) were used, and all shown spectra display the contributions from all targets. The target was surrounded by the 4π Crystal Ball detector [18] consisting of 160 NaI crystals for detecting photons and light particles emitted at laboratory angles larger than ±7° relative to the beam axis. Position and energy loss of the beam and fragments behind the target were measured by two silicon-strip detectors before deflection in the large-gap dipole magnet ALADIN. Two further position measurements behind the magnet using scintillating fiber detectors [19,20] allowed for tracking of the ions through the dipole field. Together with time-of-flight and energy-loss measurements, this provides the magnetic rigidity and atomic number and thus the mass of the fragments.

Neutrons from the decay of unbound states were detected at a distance of around 12 m downstream of the target by the LAND neutron detector [21] with an efficiency of 92% for single neutrons and with an angular acceptance of ±79 mrad around the beam axis. A similar experimental setup and analysis scheme is described in Ref. [22] in more detail.

III. ANALYSIS AND RESULTS

A. ^{25}O ground-state resonance

From the measurements of the momenta of outgoing fragments and neutrons, the two- and three-body relative-energy ($E_{\rm rel}$) spectra are reconstructed for one- and two-neutron events. Figure 1 shows the $^{24}\mathrm{O} + n$ $E_{\rm rel}$ spectrum after proton removal from ^{26}F. A prominent peak structure is visible at about 700 keV, corresponding to the ground-state resonance of ^{25}O. The position E_r and width Γ of the resonance have been extracted by fitting a Breit-Wigner distribution with an energy-dependent width using the function [23]

$$f(E; E_r, \Gamma) = \frac{\Gamma}{(E_r + \Delta - E)^2 + \Gamma^2/4}, \qquad (1)$$

with the resonance shift Δ set to zero and the width given by $\Gamma = 2P_l(E; R) \times \gamma^2$ with the reduced width amplitude γ and the penetration factor P_l. The penetration factor (taken from Ref. [24]) depends on the channel radius R, the energy E,

*t.aumann@gsi.de
†Present address: TRIUMF, 4004 Wesbrook Mall, Vancouver, BC, Canada V6T 2A3.

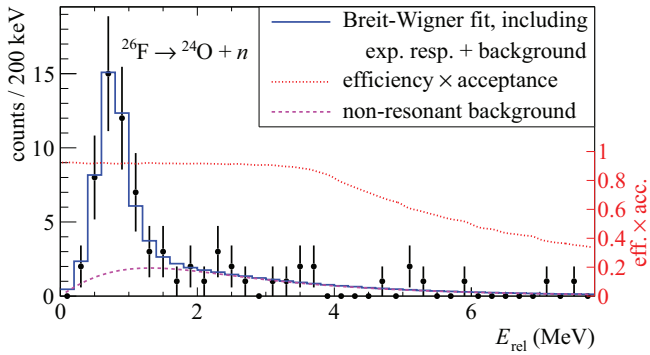

FIG. 1. (Color online) Relative-energy spectrum of the $^{24}O + n$ system measured in a proton-knockout reaction from ^{26}F. The blue solid line shows a Breit-Wigner fit to the data, which includes the experimental response and a nonresonant background (purple dashed curve). The red dotted curve indicates the experimental efficiency including the acceptance.

and angular momentum l. As the distribution was found to be insensitive to changes in R between 3.5 and 6 fm, a channel radius of 4 fm was used. An angular momentum of $l = 2$ is used, because the additional neutron of ^{25}O compared to ^{24}O is most likely in the $0d_{3/2}$ orbital.

This distribution has been convoluted with the experimental response. A nonresonant background (BG) has been modeled as the product of an error and of an exponential function,

$$f(E) = a \times \mathrm{erf}(bE) \times e^{-cE}, \qquad (2)$$

with free paramters a, b, and c. The sum of the convoluted Breit-Wigner and BG functions was used to fit the experimental data.

For the χ^2 minimization procedure, Pearson's χ^2 method [25], using errors of the parent distribution according to a Poisson probability distribution, has been used, as the usual method with errors estimated from the number of counts gives inaccurate results in case of low statistics. The extracted position (width) of $E_r = 725^{+54}_{-29}$ keV ($\Gamma = 20^{+60}_{-20}$ keV) is in agreement with the previously reported value [6] within 1σ (2σ); see Table I. Our result is in agreement with a single-particle width $\Gamma_{sp} = 65$ keV calculated for a pure d state. The relatively large experimental error on the width is attributable to the instrumental energy resolution which dominates the apparent width; see Fig. 2. For further discussion, results from literature and the present result were averaged according to Ref. [28], resulting in $E_r = 768^{+19}_{-9}$ keV and $\Gamma = 160^{+30}_{-30}$. These values are compared in the bottom panel of Fig. 3 to the expected widths and lifetimes as a function of resonance energy for different neutron angular momenta l (adopted from Fig. 2(b) of Ref. [16]). We note that the averaged width is close to the estimated value for a d state, as given in Ref. [16].

B. ^{26}O ground-state resonance

The experimental E_{rel} spectrum for ^{26}O is shown in Fig. 4, where ^{24}O has been detected in coincidence with two neutrons. Two groups of events are observed: below 1 MeV and around 4 MeV. The experimental response, indicated by the red curve, is rather constant over the displayed energy region,

TABLE I. Compilation of experimental and theoretical results obtained in this work compared to previously published results. All energies and lifetimes are given in keV and ns, respectively. Energies are measured from the g.s. energy of ^{24}O.

	E_r	Γ	τ	Ref.
^{25}O(g.s.)	725^{+54}_{-29}	20^{+60}_{-20}	$\geqslant 8.2 \times 10^{-12}$	This work
	770^{+20}_{-10}	172^{+30}_{-30}	–	[6]
Average	768^{+19}_{-9}	160^{+30}_{-30}	$4.1^{+0.9}_{-0.6} \times 10^{-12}$	
	742	$NN + 3N +$ residual $3N$		This work
	1301/1303	USDA/B		[26]
	1002	–	–	[27]
^{26}O(g.s.)	$\leqslant 40/120$ [a]	$\geqslant 1.2 \times 10^{-10}$ [b]	$\leqslant 5.7$ [c]	This work
	150^{+50}_{-150}	–	–	[13]
	40	$NN + 3N +$ residual $3N$		This work
	501/356	USDA/B		[26]
	21	0.02	–	[27]
^{26}O(e.s.)	4225^{+227}_{-176}			This work

[a] 68%/95% c.l.
[b] From lifetime estimate, see text and Fig. 3.
[c] 95% c.l.

but exhibits a steep falloff for energies below 500 keV. For such small relative energies, the neutrons are not well separated in space and time when interacting in the detector and can thus hardly be distinguished from $1n$ events. The effect can be seen quantitatively in the two-dimensional response matrices shown in Fig. 5. The energy reconstructed from the simulation is plotted versus the generated one in the top panel, showing a band along the diagonal with a width reflecting the instrumental resolution, which is shown in Fig. 2. For low generated relative energies ($\lesssim$100 keV), the events spread to a higher reconstructed energy and are, in addition, reconstructed as $1n$ events with a large probability. This can be seen in the bottom panel of Fig. 5, which shows the reconstructed $^{24}O + n$ relative energy spectrum for the events falsely identified as $1n$ events (owing to either the effect discussed above at low relative energies or to limited coverage of the detector for high relative energy). The simulation is based on measured real $1n$ events from deuteron breakup reactions. The $2n$ events are generated by overlaying the shower patterns of secondary

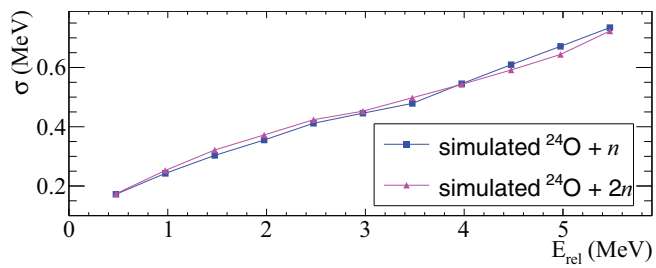

FIG. 2. (Color online) Resolution (σ) as a function of the relative energy (E_{rel}). The simulated response matrices, as shown in Fig. 5 for the $2n$ case, have been used to determine the resolution for the individual E_{rel} values.

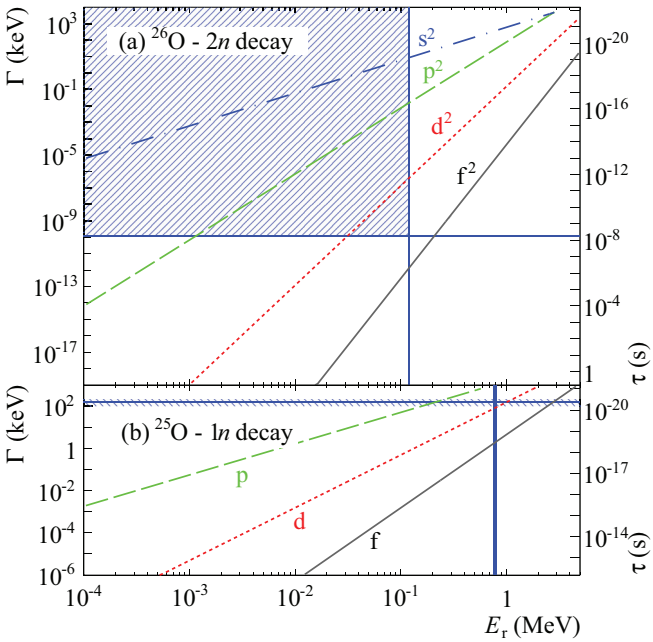

FIG. 3. (Color online) Width and lifetime as a function of resonance energy for ^{26}O (top panel) and ^{25}O (bottom panel). The curves show theoretical expectations for different l values of the neutron(s) from Ref. [16]. For ^{26}O, the (2σ) upper limits for the resonance energy and lifetime are given by horizontal and vertical blue lines. The allowed region defined by these limits is represented by the hatched area. For ^{25}O, the average of the present experiment and of the results from Hoffman *et al.* [6] is given by the horizontal and vertical blue lines, with the line thickness (hatched zone) corresponding to 2σ errors.

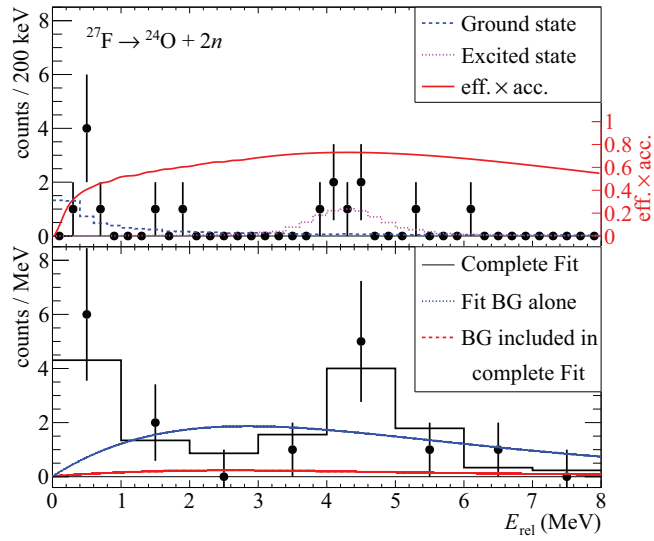

FIG. 4. (Color online) Two-neutron channel measured in coincidence with ^{24}O after one-proton removal from ^{27}F. The symbols with error bars represent the measured ^{24}O + 2n three-body relative-energy spectrum. (Top panel) The red curve displays the experimental detection efficiency including acceptance for the 2n channel; the dotted and dashed histogram shows the most probable fit to the data including two states in ^{26}O at 25 ± 25 keV and around 4 MeV. (Bottom panel) The symbols show the same data with a 1-MeV bin size; the black solid line displays a fit to the data including two resonances and a BG (red dashed curve); the blue dotted curve shows a fit using only a nonresonant BG (see text for details).

particles from these measured 1n events according to the simulated positions on the neutron detector and are then analyzed in the same way as the experimental data [29]. The generated response matrices thus do not rely on a simulation of the reactions in the neutron detection process.

The effect discussed above is clearly visible in the ^{26}O data of Figs. 4 and 6. In this 1n channel (Fig. 6), the accumulation of events at very low energy in the first bin is compelling. This feature is not present in the 1n events measured in the proton knockout from ^{26}F, as seen in Fig. 1. The events in the first bin of the ^{24}O + n spectrum are the characteristic fingerprint of a very low-lying state in ^{26}O. The events with energies above 0.2 MeV can be attributed to several processes, such as a possible direct two-nucleon knockout reaction. In particular, the events between 0.2 and 2 MeV could result from pn knockout from ^{27}F populating the ^{25}O ground-state resonance, shown in Fig. 1. At higher energies, 2n-decay events can contribute owing to the limited detector acceptance. According to the simulation, three counts are expected in the 1n spectrum between 0 and 5 MeV stemming from the resonancelike structure in the 2n channel at 4 MeV. In addition, knockout of more deeply bound protons is expected, yielding higher excitation energies in ^{26}O, which will appear as a broad BG in the 1n spectrum.

We have performed a simultaneous statistical analysis of 1n and 2n coincidences, starting with the hypothesis of a low-lying state in ^{26}O. The dotted histograms in Fig. 4 (top panel) and Fig. 6 display the most probable result, yielding a position for the ^{26}O ground state of 25 ± 25 keV. Again, the χ^2 minimization using Poisson distributed errors of the response function has been used. The response functions have been used to approximate the line shape.

Another method [30], which is independent of the binning of the experimental data, is to use the measured relative energy in each event in conjunction with the transposed response matrix to calculate the probability distribution of the true energy (Bayesian approach with uniform prior). The resulting Bayesian interval runs from 0 to 40/120 keV at a 68%/95% confidence level (c.l.). Again, both the 1n and 2n data are considered simultaneously.

We cannot exclude a very small value close to zero for position and width from the energy measurement alone, potentially leading to a rather long-lived ^{26}O ground state, which would constitute the first case of neutron radioactivity as speculated in Ref. [16]: As can be seen from Fig. 3, the lifetime for a d^2 state could reach seconds for a resonance position well below 1 keV. Such a long lifetime, however, can be excluded from the fragment measurement. The distance of the target to the middle of the dipole magnet measures 256 cm, corresponding to a flight time of 11.8 ns. If ^{26}O would decay after that time, a fragment mass greater than 24 would be reconstructed by the tracking procedure. Also, no neutron coincidences should be observed in that case, because the fragment is bent by 7° after passing half of the dipole field.

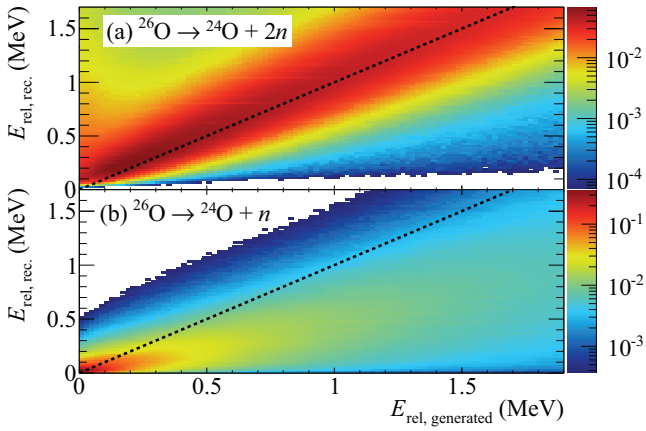

FIG. 5. (Color online) Simulated instrumental response for detection of a 2n decay of ^{26}O with relative energy E_{rel}. The top panel shows the reconstructed energy $E_{\mathrm{rel,rec.}}$ for two detected neutrons in coincidence with ^{24}O, while the bottom panel shows the $^{24}\mathrm{O}+n$ relative-energy spectrum for events, in which only one neutron has been detected owing to the limited efficiency or acceptance of the detector or owing to the multineutron recognition efficiency. $E_{\mathrm{rel,generated}}$ refers to the initial energy used as input to simulate the decay and $E_{\mathrm{rel,rec.}}$ is the reconstructed energy after simulation and analysis.

To obtain an upper limit on the number of events belonging to the previously described event class ($A > 24$ and no neutron in coincidence), the fragment mass spectrum has been inspected under the condition that no neutron is detected in coincidence; i.e., the neutron detector was used as a veto (the efficiency to detect a neutron at forward direction is 92%). The reaction trigger was provided by the Crystal Ball (CB), because for the case of proton knockout reactions, the knocked-out proton is detected at large angles with high probability in the CB. This is not only the case for $^{27}\mathrm{F}(p,2p)^{A}\mathrm{O}$ quasifree reactions on the hydrogen in the CH_2 target, but also for knockout reactions induced by composite targets. The resulting fragment-mass distribution for incoming ^{27}F and outgoing oxygen isotopes ($Z = 8$) is compared in Fig. 7 for the described trigger condition with the distribution obtained with neutron coincidences. As can be seen by comparing the

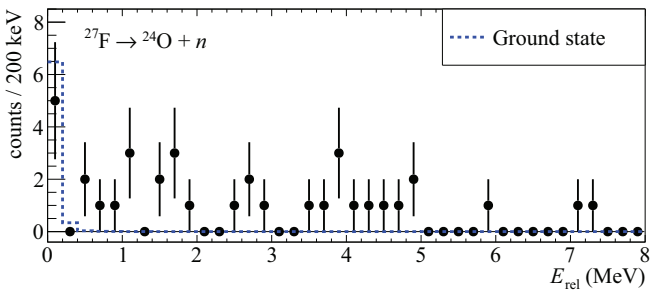

FIG. 6. (Color online) One-neutron channel measured in coincidence with ^{24}O after one-proton removal from ^{27}F. The data points represent the measured $^{24}\mathrm{O}+1n$ two-body relative-energy spectrum. The blue dashed curve displays the 1n contribution of the most probable fit to the 1n and 2n data for the ^{26}O ground state at 25 ± 25 keV, to which the 5 counts in the first bin at 100 keV are attributed (see text).

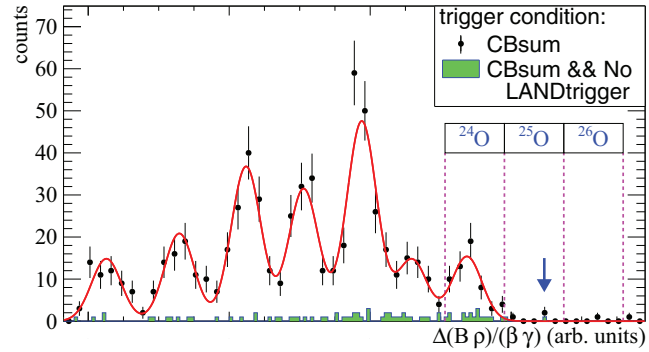

FIG. 7. (Color online) Fragment mass distribution for incoming ^{27}F and outgoing oxygen isotopes ($Z = 8$), obtained by tracking the fragment through the magnetic field. The gates for ^{24}O, ^{25}O, and ^{26}O are indicated by the vertical dashed lines. The spectrum generated by requiring the CB-sum trigger is shown as the black data points. Applying the condition that no neutron is detected in coincidence, the green histogram remains, in which one event is visible in the ^{25}O oxygen gate (indicated by the blue arrow).

two distributions in Fig. 7, there are only very few events observed without coincident neutrons, which can be explained by the neutron detection efficiency of 92% and by a small amount of BG events. Only one event appears above the ^{24}O mass, which could be attributed to BG (because there are also few events in that mass range with neutron coincidences). This one count, however, provides an upper limit on the survival probability of ^{26}O. Assuming a Poisson distribution, an expectation value of 4.9 would yield a probability of >95.5% (2σ) to detect more than one event. From the analysis of the energy spectra discussed above (see Fig. 4), the number $N(t = 0) = 20.5$ of produced ^{26}O in the ground state can be estimated. From the initial number of ^{26}O, the upper limit $N(t = 11.8\ \mathrm{ns};\ 2\sigma) = 4.9$ of surviving ^{26}O ions and the corresponding time of flight, we obtain an upper limit for the lifetime of 5.7 ns at a 95% confidence level. The upper limits for the energy of the state and for its lifetime are shown in Fig. 3, delimiting the shaded area as the allowed region, which overlaps with the calculated values for a pure d^2 state. A more complex ^{26}O ground-state configuration, however, cannot be excluded.

It would, therefore, be very interesting to determine the lifetime experimentally more precisely to gain insights on the structure of ^{26}O. Such a measurement would be rather straightforward using a similar method as described here, but placing the target directly in front of the dipole. The decay curve of ^{26}O would translate into a fragment-mass distribution depending on the decay position. In addition, the neutrons will be detected not only at 0°, but also in the bending direction, again directly reflecting the decay curve. With the intensities available, e.g., at the RIBF facility at RIKEN, a precise value could be obtained from such an experiment with the SAMURAI setup.

C. Comparison with shell-model calculations

We compare the ground-state energies of ^{25,26}O to theoretical shell-model calculations based on chiral effective

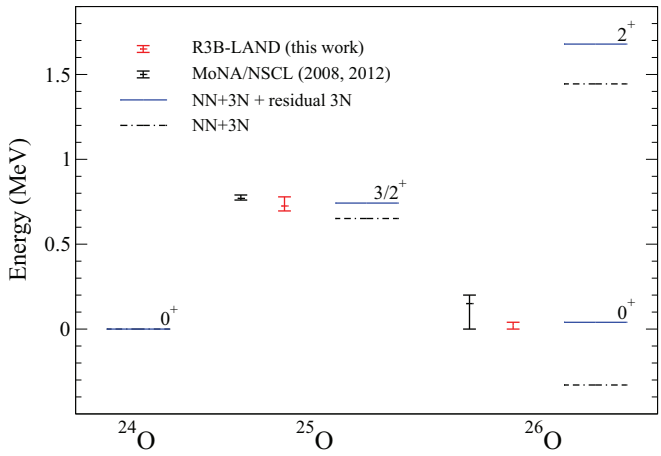

FIG. 8. (Color online) Comparison of the experimental ^{25}O and ^{26}O energies with theoretical shell-model calculations based on chiral *NN* and 3*N* forces (*NN* + 3*N*) and including residual 3*N* forces. Note that the contribution from residual 3*N* forces is 0.1 MeV in ^{24}O. The data labeled as MoNA/NSCL are from Refs. [6,13].

field theory potentials combined with renormalization-group methods to evolve nuclear forces to low-momentum interactions [31]. Our results are based on chiral *NN* and 3*N* forces, where the single-particle energies and two-body interactions of valence neutrons on top of a ^{16}O core are calculated following Refs. [32,33] without adjustments. Figure 8 shows the predicted ground-state energies obtained by full diagonalization in the valence shell $H_{NN+3N,2b}|\Psi_{NN+3N,2b}\rangle = E_{NN+3N,2b}|\Psi_{NN+3N,2b}\rangle$. In addition to the 3*N* contribution to single-particle energies and two-body interactions of valence neutrons, obtained by normal ordering, a third contribution is given by the weaker residual three-valence-neutron forces. Here, we focus on the relative contribution from these residual forces, which become more important with increasing neutron number along isotopic chains [34]. To quantify the relative contribution from residual 3*N* forces, we use the wave function $|\Psi_{NN+3N,2b}\rangle$ and calculate the correction $\Delta E_{3N,\mathrm{res}} = \langle\Psi_{NN+3N,2b}|V_{3N,\mathrm{res}}|\Psi_{NN+3N,2b}\rangle$. The repulsive contribution increases from 0.1 to 0.4 MeV for $^{24\text{–}26}$O. Because the ground states of ^{25,26}O are very narrow, thus quasibound, they can be treated fairly well in a bound-state approximation. The remarkable agreement with experiment should, however, be considered with caution, as the continuum needs to be included. The expected contribution is about 200 keV to both ^{25,26}O [35], so relative energy differences will be smaller. We have also explored uncertainties in the calculation of the single-particle energies and valence interactions, which would increase the ground-state energy relative to ^{24}O for ^{25,26}O by 0.2–0.3 MeV. In Table I, we also compare with the phenomenological USDA/B interactions [26], which predict too high energies for ^{25,26}O. Better agreement is found in Table I for the continuum shell model [27] and in recent coupled-cluster calculations with 0.4 and 0.1 MeV for ^{25}O and ^{26}O, respectively [35].

D. ^{26}O excited state

We now turn back to the group of events around 4 MeV in Fig. 4, which we interpret as resulting from the population of an excited state in ^{26}O.

Assuming first that all events above the ground state could be explained by a nonresonant BG [Eq. (2)], this yields a fit to the data in the 1- to 8-MeV range as shown in Fig. 4 (bottom) by the blue dotted curve. The probability that the observed number of counts in the 4- to 5-MeV bin are explained by this fit—yielding an expectation value of 1.60—is less than 0.018. In turn, the probability that the accumulation of events in this energy region corresponds to a peak is larger than 98% ($\approx 2.5\sigma$ significance) even in a worst case scenario.

The use of a more realistic description of the data which includes three contributions (one from the ^{26}O ground-state resonance, another from an excited state around 4 MeV, and a third contribution for the BG) results in the fit to the data as displayed by the black solid line in Fig. 4 (bottom), which represents the fit function integrated over the experimental bin width. The contribution of the BG to the total fit is shown by the red dashed line, resulting in a probability of 1.2×10^{-6} for the events between 4 and 5 MeV to belong to the BG, which is equivalent to a significance of 4.85σ for a peak structure.

The theoretical calculations based on chiral *NN* and 3*N* forces predict a first excited 2^+ state in ^{26}O at 1.6 MeV above the ^{26}O ground state. It is found at 1.9/2.1 MeV for USDA/B interactions and at 1.8 MeV for Ref. [27]. Experimentally, the events at 4 MeV in the three-body energy spectrum (Fig. 4) provide an indication for an excited state in ^{26}O, with a most probable energy of 4225^{+227}_{-176} keV. As for the ground-state resonance, the response functions have been used to approximate the line shape. The minimum χ^2 corresponds to the energy bin from 4200 to 4250 keV, which is shown in Fig. 4, including the experimental response. The errors have been determined from the χ^2 distribution using the interval given by $\chi^2_{\mathrm{min}} + 1$.

A likely candidate would be a proton-hole state populated after knockout from the ^{27}F $0p_{1/2}$ shell (rather than from the $0d_{5/2}$ valence orbital). To investigate proton (and neutron) cross-shell excitations, we have carried out $(0+1)\hbar\omega$ calculations in the *spsdpf* space using the WBP interaction [36], for which the first and second 2^+ energies are located at 2.3 and 5.4 MeV, respectively. The first state with a proton excitation component from $0p_{1/2}$ to $0d_{5/2}$ is a 3^- state at a higher energy of 5.4 MeV. Its proton contribution is also mixed with neutron excitations and considerably weaker than for the corresponding 3^- state at 5.0 MeV in ^{18,20}O. Note that ^{26}O is bound by 1.0 MeV for the WBP interaction, such that 1 MeV uncertainties are possible and the continuum should be included. The lowest negative parity states predicted by the WBP interaction are a quartet of $3^-, 2^-, 1^-, 0^-$ neutron excitations from $0d_{3/2}$ to $1p_{3/2}$ at 3.7, 4.1, 4.5, 4.9 MeV (with centroid at 4.1 MeV). A conclusion on the character of the resonancelike structure around 4 MeV in the experimental spectrum cannot be drawn from the present study. A high-statistics experiment, which would allow for an investigation of the correlations in the three-body decay, is necessary to shed light on the structure and quantum numbers of this state.

IV. COMMENT ON THE ^{26}O LIFETIME

During the final stages of the refereeing process two Letters were published in Physical Review Letters discussing the lifetime of ^{26}O, one experimental [37] and the other theoretical [38]. In the experimental work by the NSCL-MoNA group, a half-life $T_{1/2} = 4.5^{+1.1}_{-1.5}(\text{stat}) \pm 3(\text{syst})$ ps has been extracted, corresponding to a lifetime of 6.5 ps. At an 82% confidence level, a finite lifetime of the ^{26}O ground state is claimed [37], suggesting the possibility of two-neutron radioactivity. Our upper limit of 5.7 ns (95% c.l.) is in agreement with this finding. Even the combination of both results does not allow for a firm conclusion (5σ signal) on the possibility of neutron radioactivity. It is, therefore, of utmost importance to perform a dedicated and optimized experiment with good statistics to measure the lifetime of ^{26}O. With the method we have proposed in this paper, namely to measure the decay of ^{26}O in a magnetic dipole field, it will be difficult, however, to measure a lifetime shorter than 10–100 ps. The sensitivity range depends on the field strength and, in particular, on the angular resolution for the neutron detection, limiting the sensitivity with present detectors to around 100 ps, and to around 10 ps at the future R3B facility at FAIR. A more elaborated discussion of the method proposed in Sec. III B of this paper has been published in the meantime by Thoennessen *et al.* [39], together with a more detailed discussion of the method used by Kohley *et al.* [37].

The new theoretical estimate by Grigorenko *et al.* [38] implies a very low upper limit for the resonance energy of the ^{26}O ground state of around 1 keV [38], which is in agreement with the upper limit of 40/120 keV (68%/95% c.l.) as derived in the present work.

V. CONCLUSION

In summary, we have investigated the ground-state energy, width, and lifetime of the unbound oxygen isotopes ^{25}O and ^{26}O. Our results are in very good agreement with theoretical shell-model calculations based on chiral *NN* and 3*N* forces, where the ground-state energy of these extremely neutron-rich isotopes becomes increasingly sensitive to 3*N* forces among the valence neutrons. The ^{26}O ground state is unbound by less than 120 keV, and our measurement provides a limit on the lifetime of $\leqslant$5.7 ns (both at 95% c.l.). We also obtained indications for an excited state of ^{26}O located at about 4 MeV. Different possibilities for the nature of this state exist, making it an exciting case for future calculations and experiments with higher statistics.

ACKNOWLEDGMENTS

We thank B. A. Brown for helpful discussions on the WBP interaction. This work was supported by the Helmholtz International Center for FAIR within the framework of the LOEWE program launched by the state of Hesse; by the Helmholtz Alliance Program of the Helmholtz Association, Contract No. HA216/EMMI "Extremes of Density and Temperature: Cosmic Matter in the Laboratory"; by the GSI-TU Darmstadt Cooperation agreement; by the BMBF under Contracts No. 06DA70471, No. 06DA9040I, and No. 06MT238; by the DFG cluster of excellence Origin and Structure of the Universe; by US DOE Grants No. DE-FC02-07ER41457 and No. DE-FG02-96ER40963, via the GSI-RuG/KVI collaboration agreement; and by the Portuguese FCT, Project No. PTDC/FIS/103902/2008.

[1] M. Langevin, E. Quiniou, M. Bernas, J. Galin, J. C. Jacmart, F. Naulin, F. Pougheon, R. Anne, C. Détraz, D. Guerreau, D. Guillemaud-Mueller, and A. C. Mueller, Phys. Lett. B **150**, 71 (1985).
[2] D. Guillemaud-Mueller, J. C. Jacmart, E. Kashy, A. Latimier, A. C. Mueller, F. Pougheon, A. Richard, Y. E. Penionzhkevich, A. G. Artuhk, A. V. Belozyorov, S. M. Lukyanov, R. Anne, P. Bricault, C. Détraz, M. Lewitowicz, Y. Zhang, Y. S. Lyutostansky, M. V. Zverev, D. Bazin, and W. D. Schmidt-Ott, Phys. Rev. C **41**, 937 (1990).
[3] O. Tarasov *et al.*, Phys. Lett. B **409**, 64 (1997).
[4] H. Sakurai *et al.*, Phys. Lett. B **448**, 180 (1999).
[5] T. Otsuka, T. Suzuki, J. D. Holt, A. Schwenk, and Y. Akaishi, Phys. Rev. Lett. **105**, 032501 (2010).
[6] C. R. Hoffman *et al.*, Phys. Rev. Lett. **100**, 152502 (2008).
[7] R. Kanungo *et al.* Phys. Rev. Lett. **102**, 152501 (2009).
[8] K. Tshoo *et al.*, Phys. Rev. Lett. **109**, 022501 (2012).
[9] P. G. Thirolf, B. V. Pritychenko, B. A. Brown, P. D. Cottle, M. Chromik, T. Glasmacher, G. Hackman, R. W. Ibbotson, K. W. Kemper, T. Otsuka, L. A. Riley, and H. Scheit, Phys. Lett. B **485**, 16 (2000).
[10] B. A. Brown and W. A. Richter, Phys. Rev. C **72**, 057301 (2005).
[11] E. Becheva *et al.*, Phys. Rev. Lett. **96**, 012501 (2006).
[12] T. Otsuka, T. Suzuki, R. Fujimoto, H. Grawe, and Y. Akaishi, Phys. Rev. Lett. **95**, 232502 (2005).
[13] E. Lunderberg *et al.*, Phys. Rev. Lett. **108**, 142503 (2012).
[14] T. Aumann, Prog. Part. Nucl. Phys. **59**, 3 (2007).
[15] (R3B Collaboration), Technical Proposal for the Design, Construction, Commissioning and Operation of R3B, 2005, http://www-win.gsi.de/r3b/Documents/R3B-TP-Dec05.pdf.
[16] L. V. Grigorenko, I. G. Mukha, C. Scheidenberger, and M. V. Zhukov, Phys. Rev. C **84**, 021303 (2011).
[17] H. Geissel *et al.*, Nucl. Instrum. Methods Phys. Res., Sect. B **70**, 286 (1992).
[18] V. Metag, D. Habs, K. Helmer, U. v. Helmolt, H. W. Heyng, B. Kolb, D. Pelte, D. Schwalm, W. Hennerici, H. J. Hennrich, G. Himmele, E. Jaeschke, R. Repnow, W. Wahl, R. S. Simon, and R. Albrecht, in *Detectors in Heavy-Ion Reactions*, edited by W. von Oertzen, Lecture Notes in Physics Vol. 178, (Springer Verlag, Berlin, 1983), pp. 163–178.
[19] J. Cub, G. Stengel, A. Grünschloß, K. Boretzky, T. Aumann, W. Dostal, B. Eberlein, T. W. Elze, H. Emling, G. Ickert, J. Holeczek, R. Holzmann, J. V. Kratz, R. Kulessa, Y. Leifels, H. Simon, K. Stelzer, J. Stroth, A. Surowiec, and E. Wajda, Nucl. Instrum. Methods Phys. Res., Sect. A **402**, 67 (1998).
[20] K. Mahata, H. T. Johansson, S. Paschalis, H. Simon, and T. Aumann, Nucl. Instrum. Methods Phys. Res., Sect. A **608**, 331 (2009).
[21] T. Blaich *et al.*, Nucl. Instrum. Methods Phys. Res., Sect. A **314**, 136 (1992).
[22] R. Palit *et al.*, Phys. Rev. C **68**, 034318 (2003).
[23] A. M. Lane and R. G. Thomas, Rev. Mod. Phys. **30**, 257 (1958).

[24] A. Bohr and B. R. Mottelson, *Nuclear Structure* (Benjamin, New York, 1969), Vol. 1.
[25] S. Baker and R. Cousins, Nucl. Instrum. Methods Phys. Res. **221**, 437 (1984).
[26] B. A. Brown and W. A. Richter, Phys. Rev. C **74**, 034315 (2006).
[27] A. Volya and V. Zelevinsky, Phys. Rev. C **74**, 064314 (2006).
[28] R. Barlow, arXiv:physics/0401042.
[29] K. Boretzky *et al*., Phys. Rev. C **68**, 024317 (2003).
[30] P. Bevington and D. Robinson, *Data Reduction and Error Analysis for the Physical Sciences*, 2nd ed. (McGraw-Hill, New York, 1992).
[31] S. K. Bogner, R. J. Furnstahl, and A. Schwenk, Prog. Part. Nucl. Phys. **65**, 94 (2010).
[32] J. D. Holt, J. Menéndez, and A. Schwenk, Eur. Phys. J. A **49**, 39 (2013).
[33] A. T. Gallant *et al*., Phys. Rev. Lett. **109**, 032506 (2012).
[34] B. Friman and A. Schwenk, in *From Nuclei to Stars: Festschrift in Honor of Gerald E. Brown*, edited by S. Lee (World Scientific, Singapore, 2011), p. 141.
[35] G. Hagen, M. Hjorth-Jensen, G. R. Jansen, R. Machleidt, and T. Papenbrock, Phys. Rev. Lett. **108**, 242501 (2012).
[36] E. K. Warburton, J. A. Becker, and B. A. Brown, Phys. Rev. C **41**, 1147 (1990).
[37] Z. Kohley, T. Baumann, D. Bazin, G. Christian, P. A. DeYoung, J. E. Finck, N. Frank, M. Jones, E. Lunderberg, B. Luther, S. Mosby, T. Nagi, J. K. Smith, J. Snyder, A. Spyrou, and M. Thoennessen, Phys. Rev. Lett. **110**, 152501 (2013).
[38] L. V. Grigorenko, I. G. Mukha, and M. V. Zhukov, Phys. Rev. Lett. **111**, 042501 (2013).
[39] M. Thoennessen, G. Christian, Z. Kohley, T. Baumann, M. Jones, J. K. Smith, J. Snyder, and A. Spyrou, Nucl. Instrum. Meth. A **729**, 207 (2013).